Physics of Plasmas

Separating divertor closure effects on divertor detachment and pedestal shape in DIII-D

Cite as: Phys. Plasmas **27**, 032506 (2020); https://doi.org/10.1063/1.5109027
Submitted: 05 May 2019 . Accepted: 18 February 2020 . Published Online: 12 March 2020

A. L. Moser, L. Casali, B. M. Covele, A. W. Leonard, A. G. McLean, M. W. Shafer, H. Q. Wang, and J. G. Watkins

Physics of Plasmas ARTICLE scitation.org/journal/php

Separating divertor closure effects on divertor detachment and pedestal shape in DIII-D

Cite as: Phys. Plasmas **27**, 032506 (2020); doi: 10.1063/1.5109027
Submitted: 5 May 2019 · Accepted: 18 February 2020 ·
Published Online: 12 March 2020

View Online Export Citation CrossMark

A. L. Moser,[1,a),b)] L. Casali,[1] B. M. Covele,[1] A. W. Leonard,[1] A. G. McLean,[2] M. W. Shafer,[3] H. Q. Wang,[1] and J. G. Watkins[4]

AFFILIATIONS

[1]General Atomics, San Diego, California 92186, USA
[2]Lawrence Livermore National Laboratory, Livermore, California 94550, USA
[3]Oak Ridge National Laboratory, Oak Ridge, Tennessee 37831, USA
[4]Sandia National Laboratory, Albuquerque, New Mexico 87185, USA

Note: This paper is part of the Special Collection: Papers from the 60th Annual Meeting of the APS Division of Plasma Physics.
Note: Paper GI2 4, Bull. Am. Phys. Soc. **63** (2018).
[a)]Invited speaker.
[b)]**Author to whom correspondence should be addressed:** mosera@fusion.gat.com

ABSTRACT

Comparison between an open divertor and a more-closed divertor in DIII-D demonstrates detachment up to 40% lower pedestal density ($n_{e,ped}$) in the closed divertor due to a combination of decreased fueling of the pedestal and increased dissipation in the scrape off layer (SOL) in the closed divertor, both resulting from increased neutral trapping in the divertor. Predicting whether the relationship between divertor closure and detachment will hold for an opaque SOL, in which the contribution of ionizing neutrals to fueling the pedestal is lessened, requires separating out different mechanisms contributing to the density difference at detachment. A series of experiments on DIII-D characterizes matched discharges using various divertor configurations to isolate the effects of divertor closure. These experiments show detachment up to 25% lower $n_{e,sep}$ in the closed divertor than in the open divertor, supported by simulations showing increased neutral trapping, and hence, increased dissipation, in the closed divertor. A difference in $n_{e,ped}/n_{e,sep}$ is also seen: for matched $n_{e,sep}$, the closed divertor has up to 20% lower $n_{e,ped}$, consistent with modeling showing a smaller ionization fraction inside the separatrix in this case. Understanding how these pieces fit together will help in the development of predictive models of pedestal density and detached divertors compatible with a high performance core.

I. INTRODUCTION AND BACKGROUND

The need to protect plasma facing components, in particular from material erosion and damage that occur for $T_e > 5$ eV and $q > 10\,\mathrm{MW/m^2}$, requires that future tokamaks be operated in some degree of detachment. A detached divertor has a cold, dissipative divertor plasma and is characterized by a reduction in heat flux and particle flux to the divertor targets. In modern devices, divertor detachment is achieved with additional gas and/or impurity fueling to high density, which can lead to pedestal degradation and poor core performance. Future devices will require a detached divertor compatible with a high-performance core, which, in many scenarios, requires a low-collisionality pedestal, for example, to enable non-inductive current drive in a steady state.[1] Understanding how to achieve divertor detachment at a lower pedestal density in DIII-D can help us to design a future divertor in which detachment is compatible with a low-collisionality core.

Changes in divertor baffle geometry are one way in which we can affect the onset of divertor detachment,[2] by increasing the trapping of recycling neutrals near the divertor target surface. Past studies have shown the effect of changes in divertor geometry in various ways. In L-mode discharges on Alcator C-MOD,[3] a long, in-slot outer divertor leg detached at $\approx 35\% - 45\%$ lower line-averaged density, $\bar{n}_e$, than a short outer divertor leg in an open configuration. While they did not see a significant difference in $\bar{n}_e$ at detachment using the vertical in-slot target and one using a horizontal in-slot target, moving the outer strike point along the vertical target showed a nearly factor of 2 increase in $\bar{n}_e$ at detachment onset for a short leg vs a long leg. The JET tokamak compared the Mark I, Mark IIA, and Mark IIGB divertors, with the increasing closure and changing target angle of incidence.[4] It was reported that the Mark IIA divertor undergoes detachment at a lower main plasma density than the Mark I divertor; however, neutral compression rollover, which is associated with divertor detachment, was seen at ≈10% lower core plasma density in a modified version of the Mark IIA than the Mark IIGB divertor for L-mode discharges. A difference in the dynamics of detachment was seen with changing target inclination in Mark IIA, with detachment starting near the separatrix with a vertical target and farther out in the SOL for a horizontal target. Additional recent studies at JET show the effect of the target orientation on the pedestal, with the vertical target correlating with a lower pedestal density[5] and an increase in the L-H transition power threshold,[6,7] and attribute these differences to changes in the electric fields due to different T_e profiles at the divertor target. At ASDEX Upgrade, the Lyra divertor provided a more closed divertor with vertical targets at the inner and outer strike points and a central dome, compared to Divertor I with near-horizontal outer and inner divertor plates.[8,9] Experiments showed that detachment onset uniformly and near the density limit for Divertor I, and started earlier in Lyra, beginning at the separatrix and moving outwards. JT-60 compared a W-shaped divertor to an open divertor, showing that the closed W-shaped divertor detached at $10\% - 20\%$ lower $\bar{n}_e$ in L-mode and H-mode discharges.[10] DIII-D has also studied the effect of the upper closed divertor and the open lower divertor, primarily focusing on the effect of closure on core ionization but noting an ≈20% reduction in the density required for partial detachment in H-mode discharges. These studies showed that the closed divertor reduced the core ionization fraction by a factor of 2.6.[11,12]

Here, we report recent results from divertor geometry experiments at DIII-D, expanding the body of work in two key ways. First, experiments with matched shapes and conditions isolate the effects of divertor closure on detachment; in particular, we keep the outer divertor leg length and OSP angle of incidence fixed, controlling for the effect of these two parameters on detachment onset. Second, upstream pedestal profiles are used to determine the difference in $n_{e,sep}$ at detachment onset and the difference in $n_{e,ped}/n_{e,sep}$, which separates the divertor geometry effects in the SOL and those in the pedestal. This separation is important to do as future devices are expected to have a SOL that is opaque to neutrals, and so, any contribution made by differences in ionization inside the separatrix will not be present in future devices. Isolating different contributions not only leads to a better understanding of the effects of divertor closure but also allows us to develop better predictive power. In Sec. III, we determine differences in divertor detachment onset as a function of $n_{e,ped}$; we then show that this is a combination of two effects, both of which are related to increased neutral trapping in the divertor. The first effect is increased dissipation in the SOL, shown in Sec. IV, leading to detachment at a lower $n_{e,sep}$ value in the closed divertor case. The second effect is less ionization inside the separatrix, shown in Sec. V, leading to lower $n_{e,ped}/n_{e,sep}$ in the closed divertor case. Conclusions and discussion of the importance of these effects are given in Sec. VI.

II. EXPERIMENT SETUP

Experiments were performed on the DIII-D tokamak, making use of the upper and lower divertors to isolate the effects of the closed upper divertor geometry on divertor detachment onset and pedestal fueling. We compare two sets of matched, single-null, ELMing H-mode discharges: USN with the OSP on the ceiling for the closed divertor case and LSN with the OSP on the lower divertor shelf for the open case (see Fig. 1).

Focus in this paper is on the detachment of the outer divertor leg. Efforts were made to simultaneously match as many parameters as possible. The plasma shape is matched, as shown in Fig. 1, with a similar x-point height and poloidal angle between the outer divertor leg and the target. Plasma discharge and shape parameters for this comparison are given in Table I. A previous publication presents some initial analysis of these experiments and of a similar comparison performed at different plasma parameters, $P_{inj} = 3.0\,\mathrm{MW}$ and $I_p = 1.4\,\mathrm{MA}$.[13] The ion $B \times \nabla B$ drift direction has a significant effect on detachment onset,[14] and so, the toroidal field direction is reversed between the upper divertor and lower divertor discharges, to give the

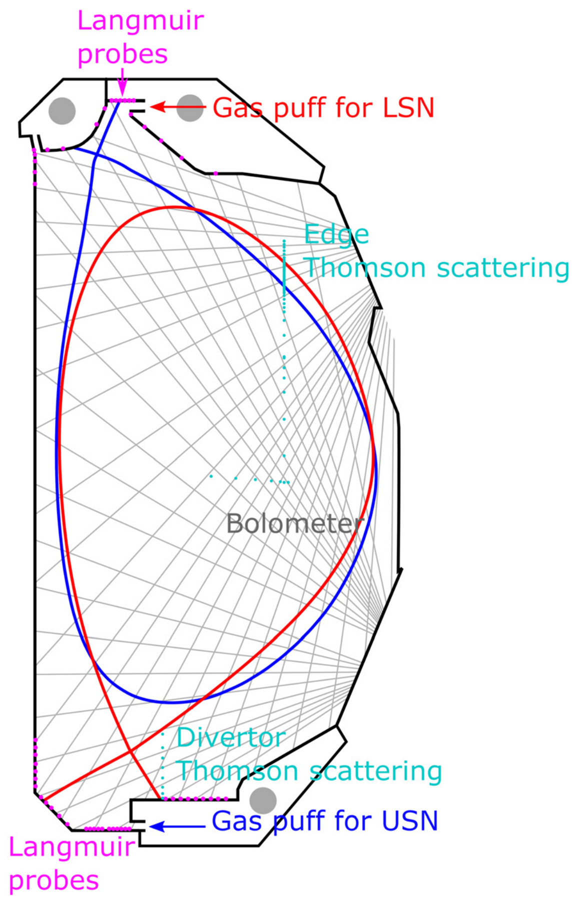

FIG. 1. We compare the upper, closed divertor (blue) with the lower, open divertor (red). In-target Langmuir probes (magenta) give J_{sat} profiles, and the edge Thomson scattering measurements (cyan) of n_e and T_e give pedestal profiles. The bolometer (gray chords) gives the two-dimensional (2D) distribution of radiated power, which is used to determine power radiated in the divertor region and is used with the pedestal profiles in power balance calculations of the separatrix location. Divertor Thomson scattering measurements (lower divertor cyan) of T_e are compared to measurements of J_{sat} rollover and $T_e \approx 2$ eV at J_{sat} rollover for this dataset. Under-baffle deuterium gas puffing locations are shown for the closed-divertor case (blue) and open-divertor case (red).

TABLE I. Plasma and shape parameters for discharges used in the detachment closure studies.

Param.	Open	Closed	Description
P_{inj}	5.6	5.8	MW, beam power
I_p	1.3	1.3	MA, plasma current
B_T	2.0	2.0	T, toroidal field
Z_x	16–19	19–22	cm, X-point height
α	113–116	123–129	deg., OSP poloidal angle with the target
κ	1.7–1.8	1.8–1.9	Elongation
δ	0.27	0.26	Triangularity (crown)

∇B drift toward the divertor in both cases. Density is controlled with deuterium gas puffing, from three toroidally separated gas valves located under the upper baffles for the LSN case and four toroidally separated gas valves under the lower baffles for the USN case. These valves provide both poloidal symmetry in the comparison, with gas puffing near the crown in both cases, and increased toroidal symmetry in each case, with multiple valve locations and the baffles allowing toroidal diffusion before gas enters the main chamber. Feed forward gas puffing is used, as response times are too long to be useful for density feedback control due to the gas line length.

The discharges are well-matched in shape and plasma parameters, as shown in Table I, but there are some differences of note. The divertor geometry at the inner strike point differs between the open and closed configurations, but we do not expect this difference to change the onset of detachment in the outer divertor. One possible effect of different geometries would be to have different conditions at the inner strike point; however, the inner strike point detaches at a significantly lower density with the ion $B \times \nabla B$ drift direction toward the divertor in DIII-D, and so, it is detached in all but the lowest density cases here. Recent studies have shown that the inner divertor can be a source of neutrals ionized in the outer divertor,[7] but that this inner divertor source was attenuated in the case of a horizontal outer target; the details of neutral pathways in the upper divertor of DIII-D is under investigation. Though there is a difference in neutral communication between the inner strike point and the outer strike point in the two divertors due to the dome structure in the upper divertor, this is a natural result of the increased closure in the upper divertor. The divertor cryo pump location and pumping efficiency vary between the upper and lower divertor cases, as shown in Fig. 1. The closed upper divertor has particle pumping in the SOL of the outer divertor leg; the pump shown under the inner dome was not used in these experiments. The open lower divertor has particle pumping in the private flux region, leading to less particle removal in the outer divertor leg than in the upper outer divertor leg. The effects of particle pumping on detachment in the upper divertor are discussed in Sec. III. The gas puff rate required to reach a given pedestal density is greater in the closed divertor, which has more effective particle removal. Despite the difference in the puff rate and pump rate, we expect the particle removal rate to balance out the particle input rate in a steady state, and so, we focus on the interrelationship between upstream values and target values, regardless of the puff rate or pump rate required. Finally, the edge Thomson scattering system is closer to the upper divertor than the lower divertor. This means that the midplane profiles are closer to the gas puff in the open divertor case than the closed divertor case. We assume that there is no direct effect of the gas puff on points inside the separatrix where we use the Thomson measurements, but it remains a possible contributor to the differences seen between the two cases.

To determine the detachment onset, a shot-wise density scan is performed, with each plasma discharge having an approximately constant density and density increasing from shot to shot; for example, time traces for a LSN discharge are shown in Fig. 2. This insures sufficient inter-ELM time for pedestal analysis at each different density. For this comparison, we use rollover in the peak ion flux to the target, J_{sat}, as a function of pedestal top density, $n_{e,ped}$, as our comparison metric for detachment onset; note that the location of that peak moves away from the separatrix as the discharge proceeds.[13] Analysis uses $200-700$ μs time windows during steady pedestal conditions and

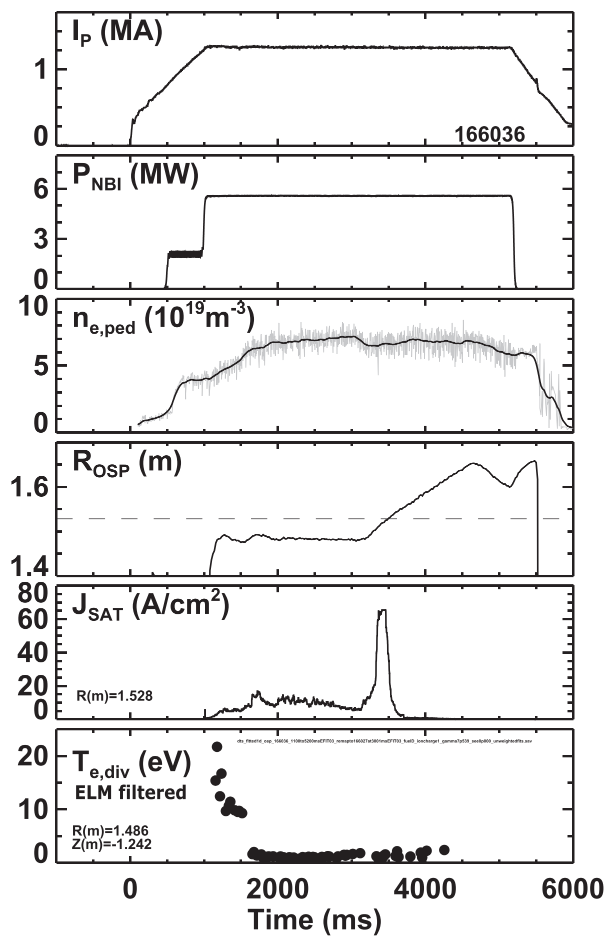

FIG. 2. Example time traces from a LSN discharge. Plasma current I_p, injected neutral beam power P_{inj}, approximate pedestal density $n_{e,ped}$, D-α emission in the lower divertor, showing ELM frequency, radial OSP position R_{OSP} showing the OSP sweep to generate profiles at the target, and ELM-filtered divertor temperature $T_{e,div}$ are shown. Time windows of 200–700 μs with steady pedestal and small OSP sweep motion are selected for analysis, which uses the last 20% of each ELM cycle.

uses the last 20% of each ELM cycle to construct an inter-ELM pedestal profile. A high-resolution edge Thomson scattering system[15] provides midplane pedestal profiles (Fig. 1), and a modified hyperbolic tangent fit gives pedestal top density, $n_{e,ped}$. For each $n_{e,ped}$, small OSP sweeps across in-target Langmuir probes generate a J_{sat} profile at the target. From this profile, we take the maximum value, peak J_{sat}. As we show in the comparison below, rollover in peak J_{sat} corresponds to the detachment of the outer divertor leg.

DIII-D has an extensive suite of boundary diagnostics, with the most comprehensive diagnostic coverage in the lower, open divertor. This includes a divertor Thomson scattering system (DTS),[16] shown in Fig. 1 that provides profiles of T_e in the lower divertor via sweeps of the OSP. Recent detachment studies in DIII-D have used $T_e \leq 2$ eV near the target as measured by the DTS as an indication of detachment. We use the overlap in coverage between DTS and in-target Langmuir probes in the lower divertor to confirm that our divertor detachment onset metric defined above captures the desired transition from attached to detached divertor conditions[13] and then use the Langmuir probe arrays in each divertor to make a direct comparison between the two configurations. Figure 3 shows a comparison between the J_{sat} rollover and T_e profiles measured by DTS in the lower, open divertor. We see that electron temperature in the lowest two DTS channels drops to $T_e \approx 2$ eV across the SOL at the rollover in peak J_{sat}. Thus, we have verified that rollover in peak J_{sat} as a function of $n_{e,ped}$ corresponds to the onset of divertor detachment for the outer divertor leg for ion $B \times \nabla B$ drift toward the divertor in DIII-D.

To accurately determine the separatrix density, we must determine the separatrix location. We use experimental measurements at the midplane and determine the separatrix position using power balance, by calculating parallel heat flux two ways and setting the separatrix to be where these two are equal.[17,18] The parallel heat flux profile is calculated assuming flux-limited Spitzer conductivity and using n_e and T_e profiles measured by the edge Thomson scattering array at the midplane. The separatrix is then determined to be the location at which this parallel heat flux matches the value calculated using the power into the SOL (P_{SOL}, based on Ohmic and auxiliary heating minus experimentally measured values of radiated power) and the SOL width. This method can shift profiles by ≈1 mm, or ≈10% of $n_{e,sep}$, compared to the more standard method of magnetic equilibrium reconstruction.[19]

We use interpretive modeling to aid in understanding results from these experiments. Calculations use experimental measurement values as input but are focused on isolating the effect of geometry in the experiment and deepening understanding of underlying effects, rather than reproducing individual discharges. We use two different codes to interpret results: SOLPS calculations focus on effects in the SOL, between the target and the separatrix, and OEDGE calculations focus primarily on effects in the pedestal, between the separatrix and pedestal top. Descriptions of simulation codes and setups used are given in Secs. IV and V.

III. COMPARISON OF DETACHMENT ONSET IN OPEN AND CLOSED DIVERTORS

Evolution of the target J_{sat} profile in the upper and lower divertors for increasing pedestal density is shown in Fig. 4. In each case, we show profiles that span the density scan from low-density, attached cases up through high-density, detached cases. These profiles show that the general shape of the ion flux to the divertor is similar in both cases and that in both cases the peak shifts outward from the separatrix with increasing density. The evolution shows the rollover in peak J_{sat}, and the density values corresponding to each profile indicate that the transition takes place at lower $n_{e,ped}$ in the closed divertor than the open in the divertor.

We can use this rollover in peak J_{sat} at the target as a function of midplane $n_{e,ped}$ as a metric for determining the detachment onset, as described in Sec. II. Using this metric to compare the detachment onset in the upper, closed divertor and the lower, open divertor shows that the closed divertor detaches at up to ≈40% lower $n_{e,ped}$ than the open divertor in these experiments. This comparison is shown in Fig. 5. A comparison to a LSN with the OSP on the floor—which we call less closed than the upper divertor, due to a lack of a private flux region baffle and a reduced outer baffle—is also shown. This intermediate closure case detaches at an intermediate $n_{e,ped}$ value between the open and closed cases and shows that progressively increasing the divertor closure increases the effect on $n_{e,ped}$ at detachment onset. A detailed study of the intermediate closure case, including investigation of the lower J_{sat} values, is left as future work. We will focus further

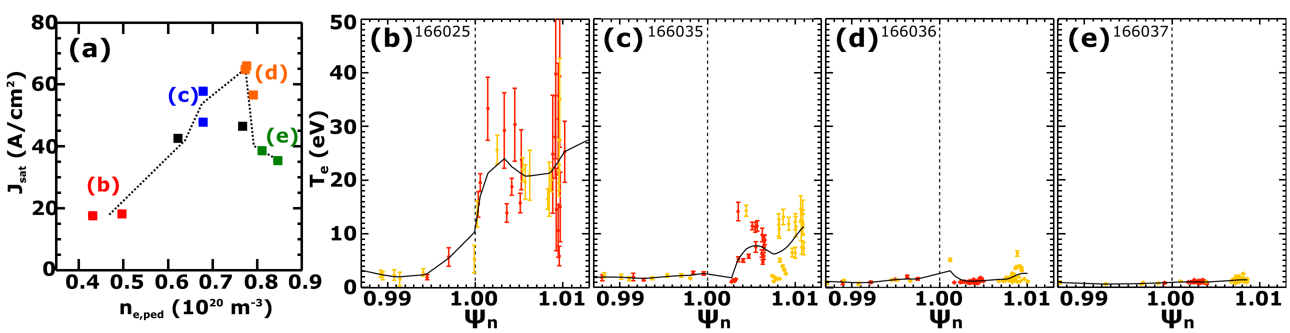

FIG. 3. Comparison between J_{sat} rollover and divertor T_e in the lower, open divertor. (a) Peak J_{sat} at the divertor target as a function of upstream $n_{e,ped}$ for the open divertor. Points corresponding to T_e measurements are indicated. (b)–(e) Electron temperature profiles in the open divertor from a chord centered ≈0.5 cm above the target (red) and ≈2.5 cm above the target (yellow). Profiles are created by sweeping the OSP past the divertor Thomson array (see Fig. 1 for measurement locations). The corresponding points from each of these four discharges are indicated in (a). Low T_e is seen only near the separatrix in (c) and is low throughout the SOL in (d). We note that although full 17 cm sweeps were used to generate the DTS profiles in (b)–(e), only a few-cm sweeps from the small-R portion of the sweep were used in the Langmuir probe analysis in (a), to minimize possible differences in target conditions due to the sweep.

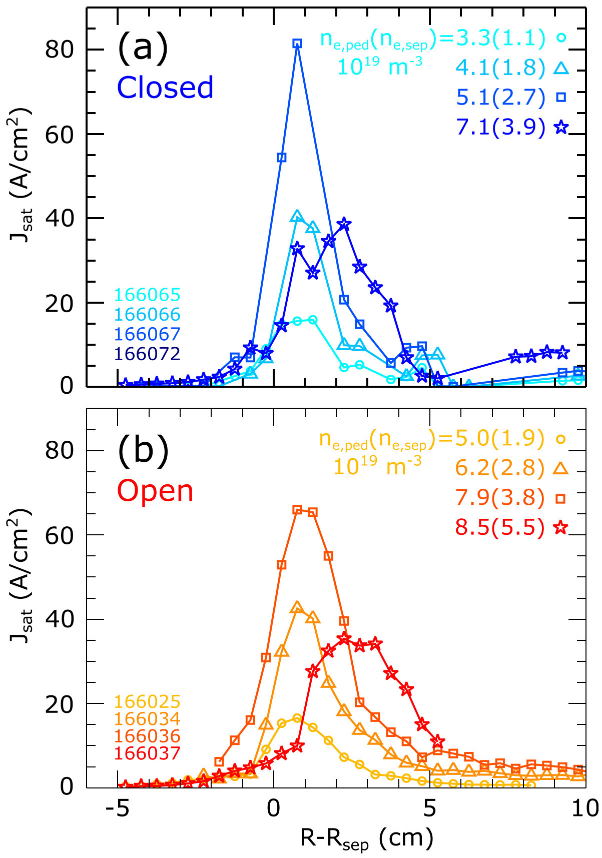

FIG. 4. J_{sat} profile evolution for the (a) closed and (b) open divertors. Each profile is from a separate discharge, generated using an ~few-cm strike point sweep. Profiles are shown for low-density attached cases (light colors), intermediate density cases, and high-density detached cases (dark colors). The peak J_{sat} value shifts outward as peak J_{sat} rolls over with increasing density.

analysis here on the open and closed cases, which show the greatest difference.

Divertor particle pumping varies between the upper and lower divertor configurations, with a pump in the SOL of the upper closed divertor and in the private flux region of the lower open divertor. This difference leads to more effective particle removal in the closed divertor configuration than the open divertor configuration. We can understand what effect this difference in pumping might have on our comparison by studying a case with pumping and a case without pumping. A comparison of detachment onset between two density ramps in the upper divertor, one with no particle pumping and one with two pumps operating, shows that the case with no particle pumping detaches at ≲10% lower $n_{e,ped}$ than the case with both pumps (Fig. 6). Note that these density ramp discharges, both pumping and non-pumping, were performed after a change in the upper divertor baffle geometry. The shape of the upper divertor was modified in 2017 to the geometry shown at top in Fig. 6; all other discharges shown in this paper used the upper divertor geometry shown in Figs. 1 and 5. The pumps and pump locations are unchanged. Only one of the two outer divertor pumps was operated in the upper divertor cases

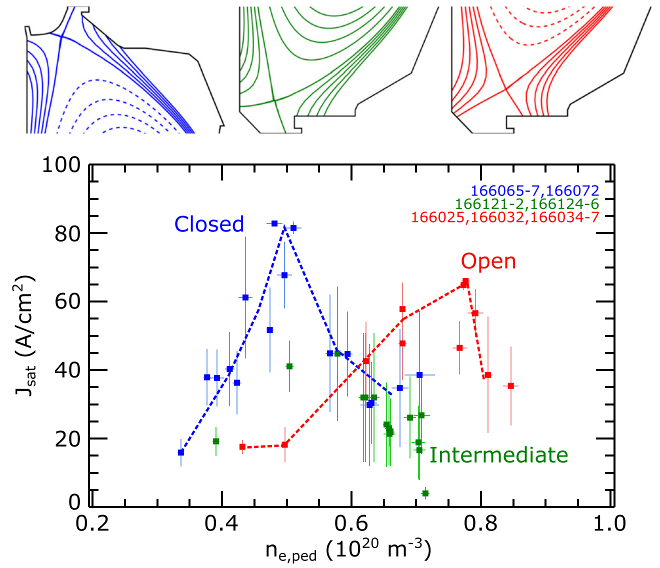

FIG. 5. Peak J_{sat} as a function of $n_{e,ped}$ for the closed (blue) and open (red) divertors, as well as an intermediate closure case with the OSP on the lower divertor floor (green). The closed divertor detaches at ≈40% lower $n_{e,ped}$ than the open divertor for this dataset. The intermediate closure divertor, with less outer divertor leg baffling than the upper divertor, falls between the two cases.

considered in this paper; it is likely that if the second pump had been used, it would have led to a bigger difference in $n_{e,ped}$ at detachment between these cases and an unpumped upper divertor case.

We see that pumping in the upper divertor can increase the $n_{e,ped}$ value required for detachment. We expect the detachment onset comparison between the open and closed configurations to be a more-conservative evaluation than if the pumping were matched, as pumping from the private flux region in the open configuration is typically weak, while the closed upper divertor has stronger common SOL pumping. More detailed analysis of the interplay between divertor closure and particle pumping is a topic of ongoing research at DIII-D.

Detachment onset determined in DIII-D conditions incorporates multiple effects between the divertor and the pedestal top, but only some of those effects will be relevant in future devices. In particular, changes in power dissipation in the SOL will contribute to detachment onset in future devices. In contrast, any contributions to the difference in detachment onset, which are attributable to changes in ionization inside the separatrix fueling the pedestal density, will be negligible in future devices, which are expected to have a main chamber SOL that is opaque to neutrals.[20,21] Separating out different effects contributing to the observed difference will therefore not only help us to better understand the effects of divertor geometry on detachment in current machines but will also allow us to better predict the effects in future machines. In Secs. IV and V, we divide the effects contributing to the ≈40% reduction in $n_{e,ped}$ at detachment into two parts: effects on the open field lines, in the divertor SOL, which lead to detachment onset at a lower $n_{e,sep}$, and effects predominantly on the closed field lines, inside the separatrix, which lead to a lower $n_{e,ped}/n_{e,sep}$.

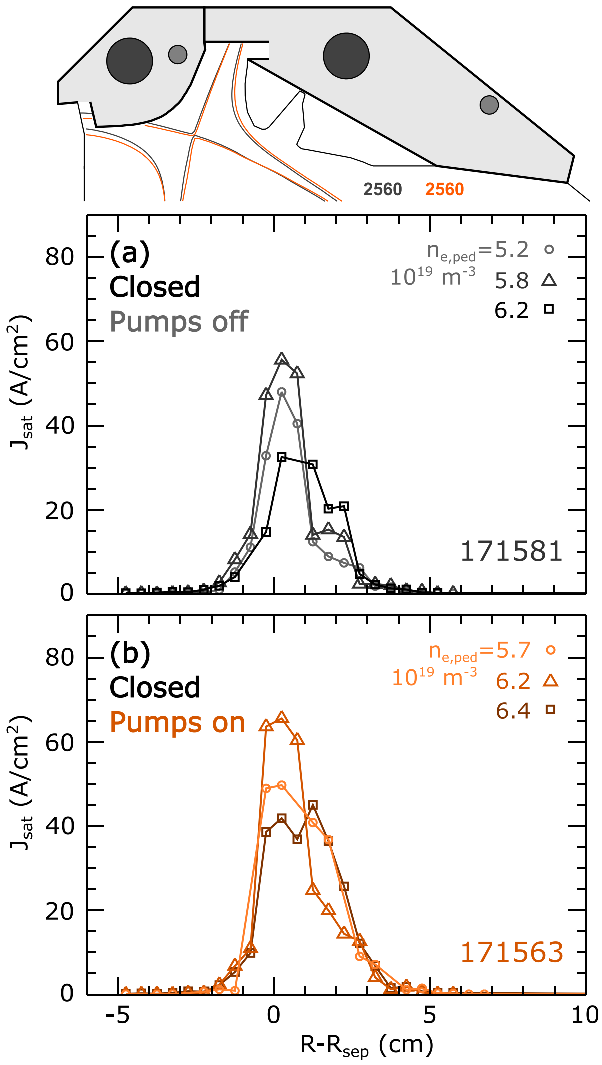

FIG. 6. The effects of particle pumping on detachment in the closed divertor. Comparison between pumping and non-pumping cases is made in the divertor geometry shown at top. Note that this upper divertor geometry is altered from other USN discharges presented here (compare geometry shown at top to divertor geometry shown in Fig. 5). (a) J_{sat} profiles for the case with pumps off. Profiles are from a single discharge with a density ramp. Profiles were chosen from a narrow density range around the peak J_{sat} rollover, which occurs near $n_{e,ped} \approx 5.8 \times 10^{19}$ m^{-3}. (b) J_{sat} profiles for the case with pumps on. Profiles are from a single discharge with a density ramp. Profiles were chosen from a narrow density range around the peak J_{sat} rollover, which occurs near $n_{e,ped} \approx 6.2 \times 10^{19}$ m^{-3}.

IV. LOWER SEPARATRIX DENSITY AT DETACHMENT ONSET DUE TO INCREASED SOL DISSIPATION IN THE CLOSED DIVERTOR

Comparing separatrix density for attached and detached divertor conditions, as determined by the metric described above, shows that the $n_{e,sep}$ value required for detachment is up to ≈25% lower in the closed divertor than in the open divertor for this dataset (see Fig. 7). This ≈25% reduction in the lowest $n_{e,sep}$ value at detachment is only a fraction of the ≈40% decrease in the required $n_{e,ped}$. Note that the error bars on $n_{e,sep}$ are fairly large, especially when density increases. Taking error bars into account, the difference between the lowest $n_{e,sep}$ values at detachment in the open and closed cases ranges from negligible to a factor of 2 difference, but the trend in the relationship between $n_{e,ped}$ and $n_{e,sep}$ for the two cases supports the conclusion that the difference is not negligible and is less than the difference seen in $n_{e,ped}$. This difference in $n_{e,sep}$ at detachment onset is due to the increased divertor and SOL dissipation for a given separatrix density in the closed divertor compared to the open divertor, which SOLPS simulations suggest is related to increased neutral trapping in the closed divertor.

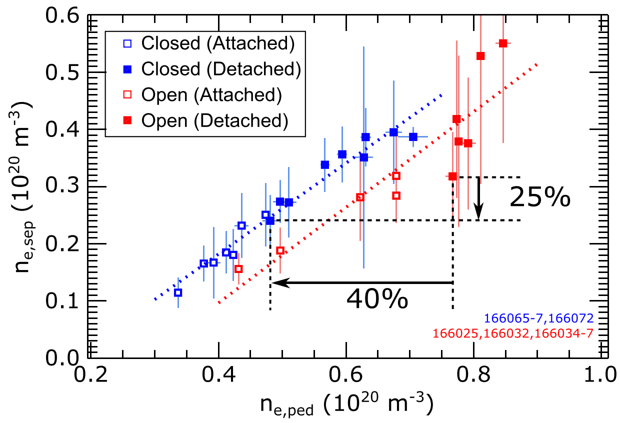

FIG. 7. Detachment as a function of pedestal density, $n_{e,ped}$, and separatrix density, $n_{e,sep}$, for the open (red) and closed (blue) divertor cases. Discharges with detached divertor conditions are indicated with filled-in symbols. Detachment in the closed divertor is seen at ≈40% lower $n_{e,ped}$, and ≈25% lower $n_{e,sep}$, than the open divertor case.

A. Setup of SOLPS simulations

We use the SOLPS (Scrape Off Layer Plasma Simulation) code suite[22] to interpret the experimental effects of geometry on the SOL plasma. SOLPS5.0 couples the multifluid plasma transport code B2.5 with the Monte Carlo neutral transport code EIRENE.[23] Computational meshes are based on experimental magnetic equilibria determined using EFIT.[24] Simulations are used in an interpretive manner, trying to understand the effects of changing geometry, rather than to reproduce specific discharges. All input parameters are kept equal between the open and closed cases in the SOLPS comparison, and only the divertor geometry is changed, allowing us to isolate the effect of divertor closure in a way that is difficult to do experimentally.

A previous publication reported results of simulations for a lower power open and closed divertor comparison,[25] and the results reported here use the same diffusion and transport coefficients with a different power. Conditions are set at the core boundary inside the separatrix; power at the boundary is based on an experimentally determined value of power into the SOL, P_{SOL}, an experimentally relevant range of n_e is used, and simulations use a zero flux boundary condition. Diffusion and transport coefficients are adjusted to reproduce the main features of experimental measurements of upstream n_e and T_e profiles in a LSN discharge;[25,26] these coefficients are then used for both divertor geometries and all densities in the comparison. SOLPS then calculates self-consistent upstream and divertor plasma conditions. Calculations include both deuterium and carbon, the latter arising from chemical and physical sputtering processes. Line emission, Bremsstrahlung, charge-exchange, elastic scattering, ionization, and recombination effects are all included. The effects of molecular deuterium are also taken into account, including molecule–ion elastic collisions and molecular assisted recombination. Drift effects, which are known to affect overall profiles and detachment characteristics, are not included, but the simulations still capture the trends expected from better neutral confinement in the divertor.

For these comparisons of the open divertor and closed divertor, density at the core boundary is varied to produce a density scan for comparison with experimental data, and diffusion and transport coefficients and power at the core boundary are held fixed between the two cases to isolate the effects of the change in divertor geometry. Full details of this modeling and the underlying physics are discussed in greater depth in Ref. 25.

B. Interpretive modeling of SOL effects with SOLPS

Interpretive SOLPS modeling of closed and open divertor discharges can indicate what differences in the SOL may be contributing to the experimentally observed difference in detachment onset. Simulations capture a similar difference in detachment onset between the open and closed divertors to that seen experimentally, with previous work at lower power showing that the closed divertor T_e drops below 2 eV at approximately 50% lower upstream density.[25] For the simulations of discharges shown here, the closed divertor reaches $T_e \approx 2$ eV at $\approx$30% lower $n_{e,sep}$ than the open divertor. We can use this SOLPS comparison to gain insights into which processes are contributing to the decrease in separatrix density required for detachment.

We expect an increase in neutral trapping in a closed divertor compared to an open divertor and that this increased trapping of neutrals can lead to more dissipation in the divertor/SOL in a closed geometry. This effect is seen in SOLPS comparisons, which show greater neutral density in the closed divertor than in the open divertor. Figure 8 shows 2D neutral distribution in the open and closed divertors for matched $n_{e,sep} \approx 0.5 \times 10^{20}$ m^{-3}, with greater neutral density throughout the closed divertor. We can see that this difference in neutrals in the closed case is due to increased neutral trapping by also comparing the neutral density at the midplane, which we expect to be lower in the closed case. Figure 9(a) shows the radial profiles of neutral density at the midplane for the open divertor configuration and the closed divertor configuration, for two different $n_{e,sep}$ values, demonstrating that the neutral density is lower throughout the midplane SOL for the closed divertor case. Figure 9(b) shows poloidal neutral density profiles along a flux surface from the divertor target to the outboard midplane for different $n_{e,sep}$ values for both the open and closed cases. For both $n_{e,sep}$ values, the closed divertor shows significantly higher neutral density in the divertor region than the open divertor and lower neutral density than the open divertor case at the outboard midplane, consistent with increased neutral trapping in the closed divertor. SOLPS shows peak neutral density to be greater in the closed divertor than the open for all $n_{e,sep}$ of the density scan,[26] consistent with past SOLPS work showing a strong inverse correlation between n_{D_2} and T_e in the divertor.[27]

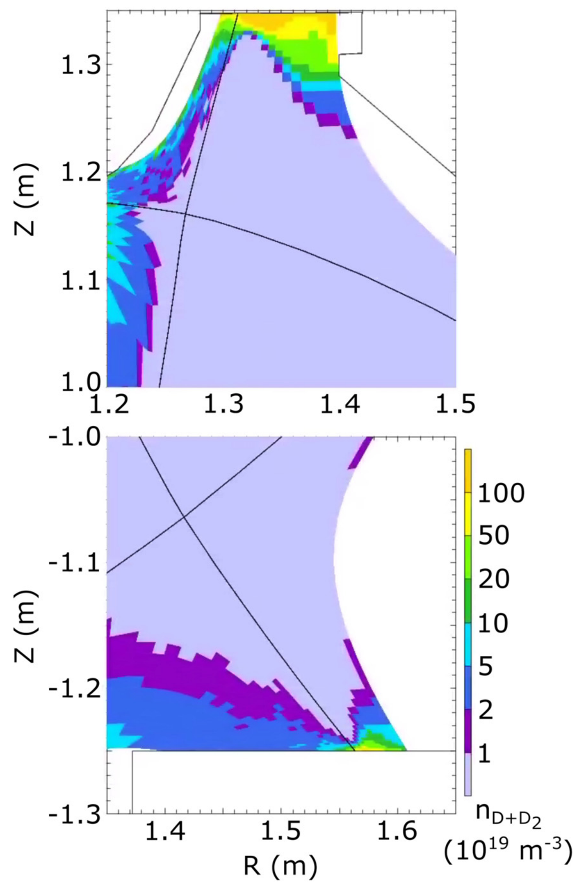

FIG. 8. Two-dimensional distribution of neutral deuterium density, n_{D+D_2}, in the closed (top) and open (bottom) divertor volume, both for $n_{e,sep} \approx 0.5 \times 10^{20}$ m^{-3}. There is a higher neutral density throughout the closed outer divertor, including at the target, which is calculated with SOLPS.

Low target temperatures in detachment are due to energy dissipation,[28] and while momentum dissipation can also be an important effect in detached divertors, we focus here on energy dissipation. Radiated power in the divertor region is a primary contributor to energy dissipation, and hence, the observation of detachment at lower separatrix density in the closed divertor indicates that the closed divertor must be dissipating more of the power that flows into the SOL than the open divertor does for the same $n_{e,sep}$. To see this, we can compare the power radiated in the outer divertor normalized by the power into the SOL, $P_{rad,divout}/P_{SOL}$, as a function of $n_{e,sep}$. Total radiated power in the outer divertor leg is measured by using the bolometer arrays shown in Fig. 1. Tomographic inversion gives a 2D radiation profile, and total outer divertor radiation is determined by summing radiating power in the SOL outboard of the x-point from the target to 20 cm above the x-point. It is then normalized by the power into the SOL, to take into account changes in core radiation with changing density. The results are shown in Fig. 10, with detached divertor conditions indicated by filled-in symbols, based on rollover in peak J_{sat} for experimental measurements and $T_e \approx 2$ eV for SOLPS simulations. The closed divertor $P_{rad,divout}/P_{SOL}$ is up to twice that of the open

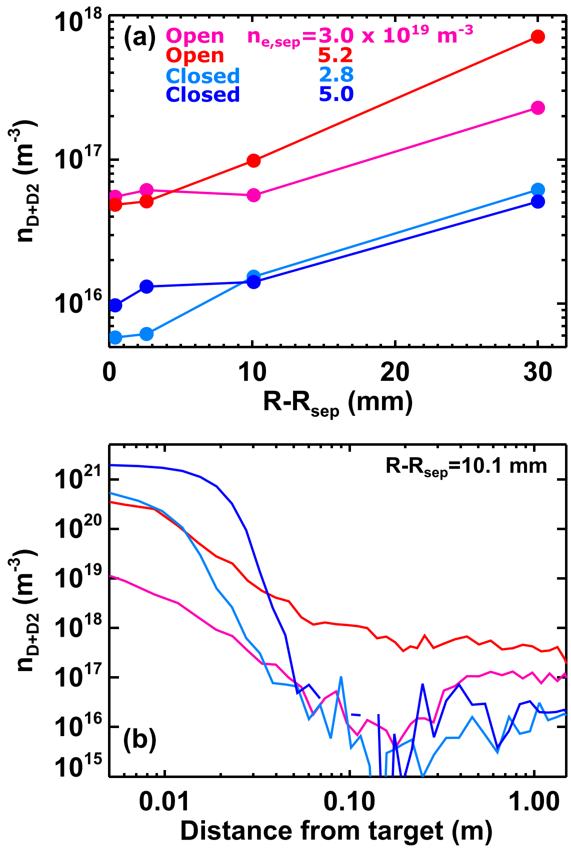

FIG. 9. Profiles of neutral deuterium density, n_{D+D_2}, calculated with SOLPS. (a) Radial n_{D+D_2} profile at the midplane, at $n_{e,sep} = 3$ and 5×10^{19} m^{-3} for the open (reds) and closed (blues) cases. (b) Poloidal n_{D+D_2} profiles at the same two $n_{e,sep}$ values for the open (reds) and closed (blues) cases. Poloidal profiles are along the flux contour with $R - R_{sep}$=10.1 mm at the outboard midplane. The closed case shows much higher neutral density near the divertor, with decrease density at the outboard midplane. This demonstrates the trapping of neutrals in the divertor.

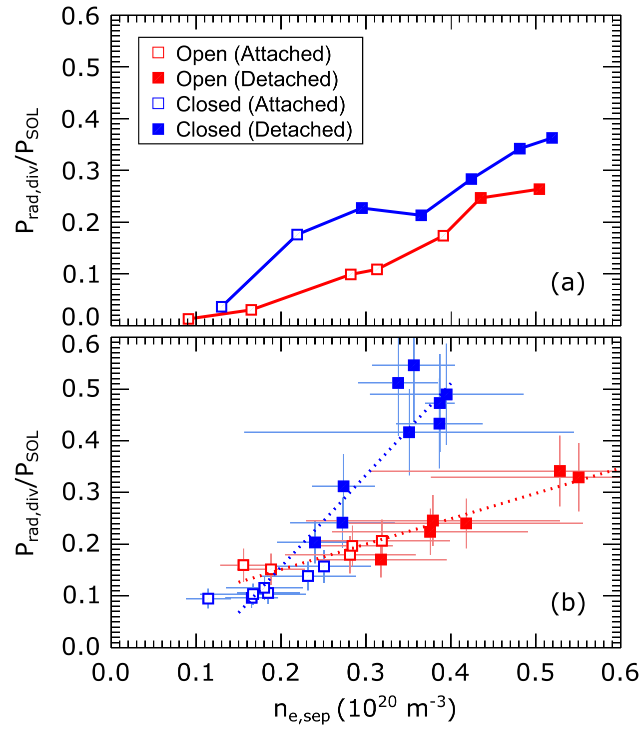

FIG. 10. Total power radiated in the outer divertor leg as a function of separatrix density. Radiated power is normalized by the power flowing into the SOL. (a) SOLPS calculated values for the open (red) and closed (blue) cases. Values are taken directly from SOLPS simulations, not calculated using a synthetic diagnostic. (b) Experimental values based on bolometer measurements for the open (red) and closed (blue) divertors. Detached divertor conditions are indicated by filled-in symbols in both cases.

divertor for the same $n_{e,sep}$ at high densities and ≈1.3 times greater at detachment onset in the closed divertor, with both divertors showing detachment onset at $P_{rad,divout}/P_{SOL} \approx 0.2$. This indicates much greater dissipation for the same separatrix density in the closed case than in the open divertor, which leads to detachment onset in the closed divertor at lower separatrix density. We discuss other sources of power loss beyond radiation below.

The SOLPS calculations of radiated power for the outer divertor are shown in Fig. 10. These SOLPS calculations capture important trends seen in the experimental data: the closed case shows greater radiation than the open case, by a factor of about 1.3 for the highest densities and a factor of 2 at detachment onset in the closed divertor. Both the open and closed cases detach at $P_{rad,divout}/P_{SOL} \approx 0.2 - 0.3$. The difference between the open and closed cases is less than that seen experimentally, which could be due to a number of factors, including factors that contribute to the absolute values being lower in the SOLPS case, a trend analyzed in detail in other studies.[29,30]

Through the analysis of SOLPS results, we find the relative contribution of dissipative processes not measured by the bolometers, like charge-exchange and other ion–neutral interactions. A comparison of the relative contributions of radiation from carbon impurities, radiation from deuterium, and ion–neutral interactions (charge exchange and other collisional dissipative losses) is shown in Fig. 11. Radiation dominates ion–neutral interactions, with carbon providing the greatest contribution in both the open divertor and the closed divertor, as has been seen in experimental measurements of divertor radiation in DIII-D.[31,32] If we were to compare the power radiated by deuterium and by carbon separately, we would see that each is greater in the closed divertor case than in the open case, but if we consider the relative contribution of deuterium and carbon we see that that the relative contribution of deuterium increases in the closed case, while the relative contribution of carbon decreases (Fig. 11). Similarly, ion–neutral interactions have almost twice the relative contribution in the closed case than in the open case. The increase in the importance of deuterium radiation and ion–neutral interactions is consistent with the greater density of deuterium neutrals in the closed divertor.

V. LOWER PEDESTAL DENSITY DUE TO DECREASED IONIZATION INSIDE THE SEPARATRIX IN CLOSED DIVERTOR

The pedestal density is up to ≈20% lower in the closed divertor case than in the open divertor case for a given separatrix density.

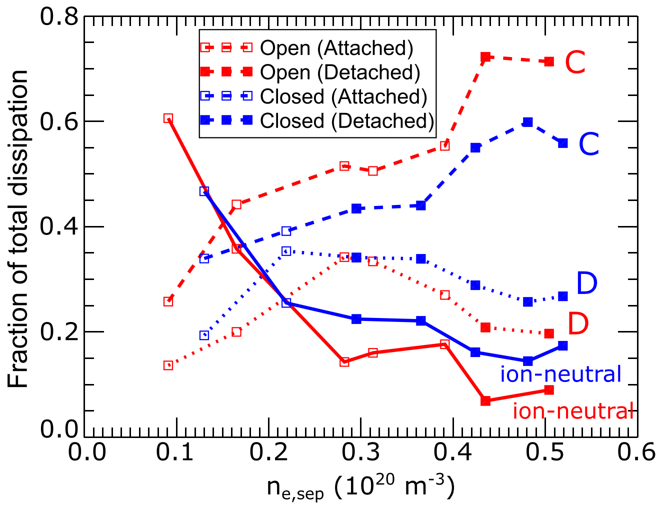

FIG. 11. Fractional contribution of different dissipative processes as a function of separatrix density. Values are calculated in the outer divertor volume, for carbon radiation (dashed lines), deuterium radiation (dotted lines), and ion–neutral dissipative processes (solid lines). The relative contributions of deuterium are larger in the closed case, consistent with greater deuterium neutral density. Values are calculated in SOLPS. Carbon and deuterium radiation together give total radiation plotted in Fig. 10. All red lines are for the open divertor case, while all blue are for the closed divertor case; detached divertor conditions are indicated by filled-in symbols.

A plot of $n_{e,ped}/n_{e,sep}$ vs $n_{e,sep}$ (Fig. 12) shows that $n_{e,ped}/n_{e,sep}$ is greater in the open divertor case for all the values of $n_{e,sep}$ in these experiments. OEDGE simulations suggest that the observed difference in $n_{e,ped}/n_{e,sep}$ is due to differences in where the recycling neutrals are ionized, which is related to the increase trapping of neutrals in the divertor discussed in Sec. IV.

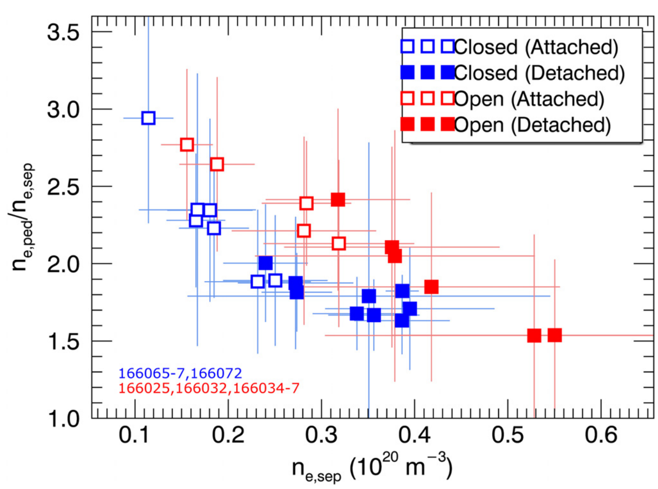

FIG. 12. Experimentally measured values of the ratio of pedestal density to separatrix density, $n_{e,ped}/n_{e,sep}$, as a function of $n_{e,sep}$, for the open divertor (red) and closed divertor (blue) cases. The closed divertor has an up to 20% lower $n_{e,ped}/n_{e,sep}$. These are the same data shown in Fig. 7, replotted to highlight $n_{e,ped}/n_{e,sep}$.

A. Setup of OEDGE modeling

To more accurately estimate the effect of geometry on the pedestal ionization source profile, we employ the OEDGE (Onion-skin modeling + EIRENE + DIVIMP for edge analysis) coupled code, which has been used in past studies of core-ionization.[33,34] This interpretive approach uses EIRENE to follow the best experimental estimate of the neutral source profile through an empirically reconstructed background plasma based on an onion-skin model. While in principle a similar interpretive analysis can be carried out with SOLPS modeling, we find the OEDGE code to be more efficient and accurate in reproducing the experimental measurements for the assessment of the deuterium ionization profile. The onion-skin modeling code produces a 2D background plasma based on experimental measurements of divertor target J_{sat} and T_e profiles measured by in-target Langmuir probes and upstream T_e and n_e pedestal profiles measured by Thomson scattering. EIRENE launches neutrals into the background plasma assuming unity recycling, with the Eirene grid extending to the walls and the plasma grid extending from the private flux region to the outer SOL. Neutrals are launched from the divertor and main chamber walls with the same profile as the ion flux to the surfaces; this is measured by Langmuir probes in the divertor and extrapolated to other surfaces using characteristic SOL lengths. Once launched, neutrals can make their way around the plasma, ionizing in both the SOL and inside the separatrix; OEDGE produces 2D profiles of the ionization rate. Calculated volume recombination is included, but the recombination source is very small for the attached divertor cases modeled. DIVIMP, an impurity neutral and ion Monte Carlo transport code, is not used here. Carbon impurities are hence not included explicitly, but the effects of carbon on radiation losses are implicitly taken into account by the experimental profile matching in the setup, as are differences in gas puffing and pumping rates.

B. Interpretive modeling of pedestal effects with OEDGE

We can compare OEDGE calculations of 2D ionization profiles for open and closed divertor discharges with matched $n_{e,sep}$ to see how divertor geometry affects the ionization profiles. Figure 13 shows the 2D ionization profiles for discharges with $n_{e,sep} \approx 0.18 - 0.19 \times 10^{20}$ m^{-3}. The outer leg of the closed divertor shows ionization occurring over a larger volume of the divertor than the outer leg in the open divertor, as well as larger overall ionization rates, and very little ionization inside the separatrix. In contrast, the open divertor shows ionization inside the separatrix that extends up toward the midplane. This is consistent with a picture of increased neutral trapping in the closed divertor: neutrals trapped in the closed divertor have more of a chance of being ionized in the SOL, whereas in the open divertor case, neutrals escape the divertor region and travel upstream, where they can more easily cross the narrow SOL and be ionized inside the separatrix.

We see this effect in the plot of ionization as a function of the poloidal angle shown in Fig. 14. Here, the ionization rate inside the separatrix has been multiplied by the radiating volume and summed in the radial direction to give a total ionization rate for a given poloidal slice. This comparison shows significantly more ionization inside the separatrix between the x-point and the midplane in the open divertor case everywhere but the immediate x-point region. Ionization is high for a small region near the x-point in the closed divertor and drops

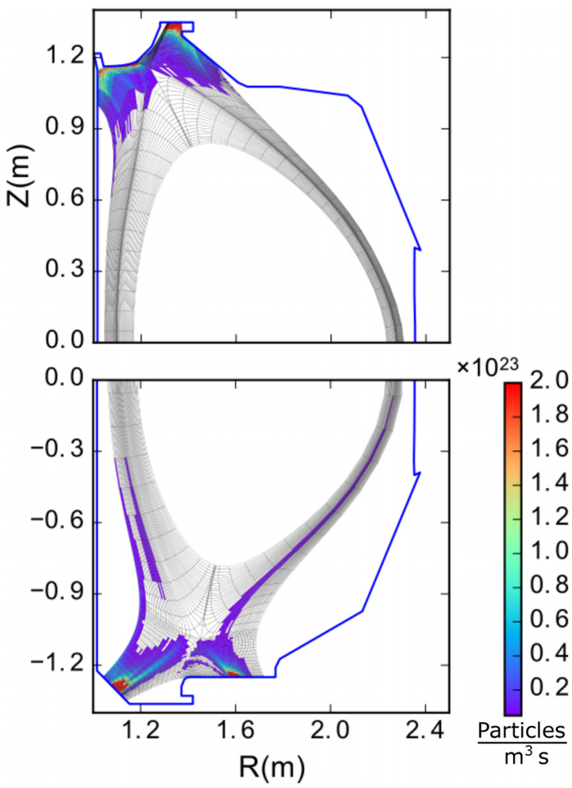

FIG. 13. Ionization rate as a function of position for the closed (upper) and open (lower) divertors, for matched separatrix density. Rates calculated with OEDGE. The closed divertor shows more ionization in the outer divertor leg than the open; the open shows more ionization outside of the divertor region, including inside the separatrix. Ionization inside the separatrix for both cases is shown in Fig. 14.

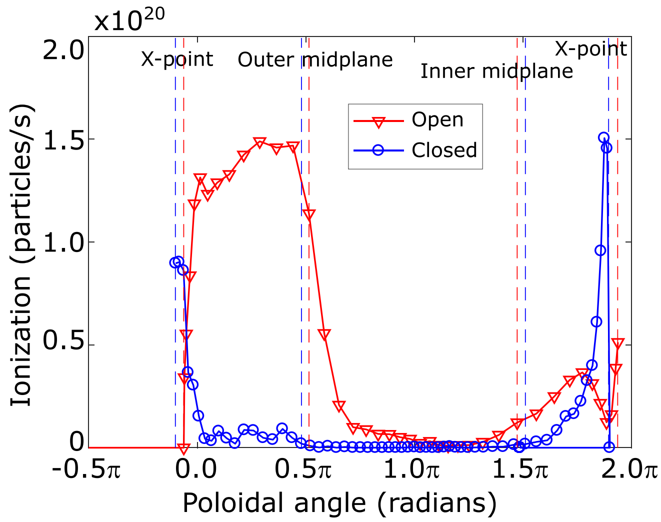

FIG. 14. Total ionization rate inside the separatrix as a function of the poloidal angle. Both cases are plotted starting from the x-point and moving toward the outboard midplane, so "clockwise" for the closed divertor (blue) and "counterclockwise" for the open divertor (red). X-point, outboard midplane, and inboard midplane positions in each case are indicated by dashed vertical lines. Rates are calculated with OEDGE and multiplied by volume to take the effect of varying volume into account. (Note that poloidal grid divisions are different in the two cases and that the sum of the values plotted, rather than the area under the curve, gives the total ionization.) The open divertor shows much greater ionization than the closed outside the immediate x-point region, with ionization peaking just below the outboard midplane.

quickly upstream, whereas in the open divertor case, ionization is high from just outside the x-point up past the midplane, peaking just below the midplane. We note that this joins previous work showing poloidal variations in the deuterium atomic flux across the separatrix,[35] though that work, which studied L-mode discharges with UEDGE and SOLPS, found varying relative contributions between regions near the x-point and regions closer to the midplane.

Comparing poloidally averaged ionization inside the separatrix for the two geometries, we find higher ionization in the open divertor case for all the values of normalized magnetic flux Ψ_n, Fig. 15(a). Ionization rates are similar just inside $\Psi_n = 1$ and diverge moving inwards, leading to a greater fractional increase in the ionization rate inside the separatrix near the pedestal top. The differences in ionization rates lead to approximately twice as much ionization inside the separatrix in the open case (1.9×10^{21} particles/s) as in the closed case (1.0×10^{21} particles/s). This is shown in the plot of radial ion flux [Fig. 15(b)], which balances out the ionization inside the separatrix and is calculated by radially integrating the ionization profile. Figure 15(b) shows that the $\approx 2\times$ increase in radial ion flux corresponds to an $\approx 2\times$ increase in the peak pedestal density gradient, $dn_e/d\Psi_n$. Though there are many processes that can affect the pedestal profile in addition to diffusion, we see with this simple empirical estimate that the pedestal fueling and the resulting gradient change by a similar factor, as is expected from standard diffusive processes. We note that these profiles are not determined self-consistently from transport models and calculated ionization rates; rather, the pedestal profiles are taken directly from measurements and used to calculate ionization rates.

The closed divertor case has more ionization in the divertor region, increasing n_e in the SOL, and the open divertor has more ionization inside the separatrix, increasing n_e in the pedestal. These differences in ionization are calculated using the observed difference in the pedestal density profile shown in Fig. 15. This is consistent with the results of a similar SOLPS comparison between lower power open and closed divertor cases that showed more ionization inside the separatrix in the open case for matched divertor target conditions.[36] These results join a body of evidence that changes in the neutral fueling have a strong effect on the pedestal structure in DIII-D, including a study showing that the pedestal width is comparable with the neutral penetration length[37] and a study of the pedestal fueling from the divertor and main chamber recycling, which found that the divertor source dominated.[38] These two studies were performed using open divertor discharges; a recent comparison of the open and closed divertors on DIII-D found differences in the pedestal height, width, and displacement, consistent with changes to differences in pedestal fueling from divertor-sourced neutrals.[39] We note that the effect of neutral fueling on the pedestal structure observed on DIII-D is not universal. Past studies on Alcator C-Mod found that the pedestal width did not vary with density as expected from a simple neutral penetration model, though they note that it is difficult to study the role of neutral fueling on the pedestal experimentally, due to changes in pedestal density

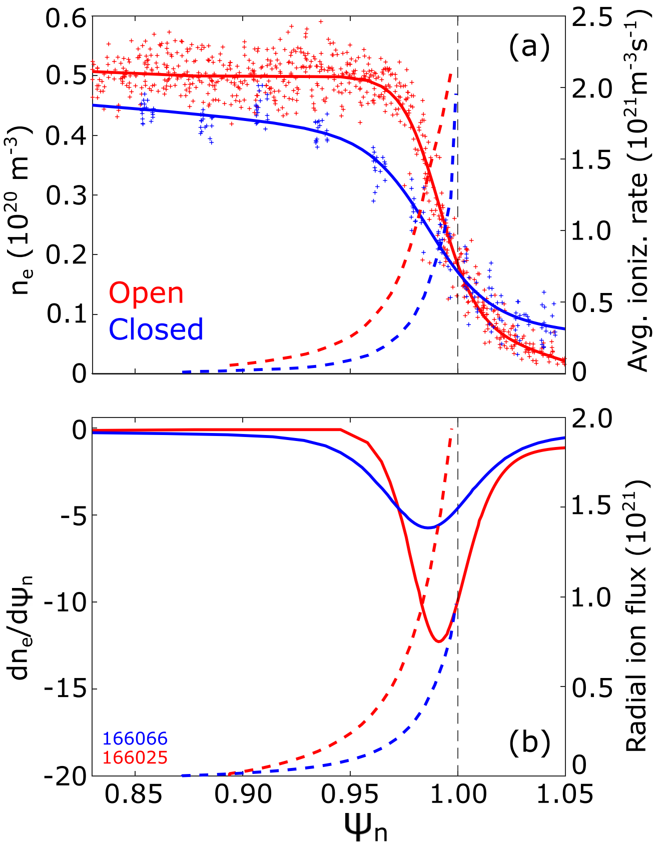

FIG. 15. Ionization rate and ion flux calculated with OEDGE for the closed (dashed blue) and open (dashed red) divertors. (a) Poloidally averaged ionization rate inside the separatrix as a function of normalized poloidal flux Ψ_n. Ionization rate is plotted over experimentally measured n_e profile. The open divertor shows greater ionization than the closed, corresponding to a higher pedestal top density. (b) Radial ion flux as a function of Ψ_n indicates a factor of 2 difference in total ionization inside the separatrix. Plotted over density gradient, $dn_e/d\Psi_n$, from fit to experimental data shown in (a). Higher ion flux corresponds to higher density gradient.

affecting radial transport.[40] A multi-machine comparison of DIII-D, ASDEX Upgrade, and JET concluded that the data suggest a role for neutral fueling in determining the density profile but that further study is needed.[41]

VI. SUMMARY AND CONCLUSIONS

Experimental measurement of detachment onset comparing the more closed upper divertor and more open lower divertor on DIII-D shows that the closed divertor achieves detachment at up to ≈40% lower $n_{e,ped}$ than the open divertor. Further analysis of experimental data indicates that this difference is a combination of two factors: detachment onset at ≈25% lower $n_{e,sep}$ in the closed divertor than in the open divertor and an ≈20% lower $n_{e,ped}/n_{e,sep}$ in the closed case than in the open case. Interpretive modeling suggests that both these factors are related to increased trapping of neutrals in the closed divertor.

Experimental measurements and SOLPS modeling of $n_{e,sep}$ scans for the two divertor configuration indicate that the onset of detachment for the closed divertor at lower $n_{e,sep}$ is due to greater dissipation in the divertor. Simulations suggest that this is due in part to greater neutral density in the closed case. Experimental measurements show a 30% increase in $P_{rad,divout}/P_{SOL}$ for the closed over open configuration at detachment onset. SOLPS modeling captures a similar trend in $P_{rad,divout}/P_{SOL}$, with an ≈2 times increase in the closed case at detachment onset. SOLPS also indicates that the contribution of deuterium radiation and ion–neutral collisional processes has a greater relative contribution to total dissipation in the closed divertor than in the open divertor, consistent with increased neutral trapping.

OEDGE calculations indicate that greater neutral trapping in the closed divertor also contributes to the observed difference in $n_{e,ped}/n_{e,sep}$. The closed geometry more effectively traps neutrals, leading to greater ionization in the divertor SOL, while the more open divertor geometry allows more neutrals to escape the divertor, cross the separatrix, and be ionized. Though some neutrals cross the separatrix near the x-point in both divertor geometries, ionization upstream is an additional pathway only available to neutrals that escape the divertor that is much more likely in the open divertor configuration. The OEDGE analysis of experimental discharges with matched $n_{e,sep}$ shows more ionization inside the separatrix in the open divertor case, leading to twice the ionization of the closed divertor case. These two trends, more ionization in the SOL in the closed case and more ionization inside the separatrix in the open case, act to modify the pedestal profile so that $n_{e,ped}/n_{e,sep}$ is greater in the open divertor case.

We do not expect significant ionization inside the separatrix in future devices;[20,21] hence, we would not expect a significant difference in $n_{e,ped}/n_{e,sep}$ between an open divertor and a closed divertor. So, the contribution of a difference in $n_{e,ped}/n_{e,sep}$ to the difference in detachment onset would be absent, leaving only the contribution of the increased SOL dissipation in the closed case. So, in the case of the comparison we make here, rather than the ≈40% decrease in density at detachment onset that we see when we look at the onset of detachment as a function of $n_{e,ped}$, we would expect to see the ≈25% decrease in density we see when we look at detachment onset as a function of $n_{e,sep}$. This is not to say that these results scale directly to future devices; rather, these results may aid in verifying models of the existing experiments to test the physics used to extrapolate to future tokamaks.

These experiments also indicate that the closed divertor geometry is more compatible with the requirement of a low-collisionality core plasma. Comparing detached cases with similar peak target ion flux values shows that the closed divertor case has a lower pedestal density but a higher pedestal temperature, leading to a lower pedestal top collisionality with a slightly higher pedestal pressure than the open case.[39] This suggests that a closed divertor geometry may help provide a future reactor with a detached divertor that still allows a low collisionality, high pressure pedestal.

ACKNOWLEDGMENTS

This material is based upon the work supported by the U.S. Department of Energy, Office of Science, Office of Fusion Energy Sciences, using the DIII-D National Fusion Facility, a DOE Office of Science user facility, under Award Nos. DE-FC02-04ER54698, DE-AC52-07NA27344, DE-AC05-00OR22725, and DE-AC04-94AL85000.

This report was prepared as an account of work sponsored by an agency of the U.S. Government. Neither the U.S. Government

nor any agency thereof, nor any of their employees, makes any warranty, express or implied, or assumes any legal liability or responsibility for the accuracy, completeness, or usefulness of any information, apparatus, product, or process disclosed, or represents that its use would not infringe privately owned rights. Reference herein to any specific commercial product, process, or service by trade name, trademark, manufacturer, or otherwise, does not necessarily constitute or imply its endorsement, recommendation, or favoring by the U.S. Government or any agency thereof. The views and opinions of authors expressed herein do not necessarily state or reflect those of the U.S. Government or any agency thereof.

REFERENCES

[1] A. Garofalo, V. Chan, J. Canik, M. Sawan, M. Choi, D. Humphreys, L. Lao, R. Prater, P. Stangeby, H. S. John, T. Taylor, A. Turnbull, and C. Wong, Nucl. Fusion **54**, 073015 (2014).

[2] A. Loarte, Plasma Phys. Controlled Fusion **43**, R183 (2001).

[3] B. Lipschultz, J. Goetz, I. Hutchinson, B. LaBombard, G. McCracken, Y. Takase, J. Terry, P. Bonoli, S. Golovato, P. O'Shea, M. Porkolab, R. Boivin, F. Bombarda, C. Fiore, D. Garnier, R. Granetz, M. Greenwald, S. Horne, A. Hubbard, J. Irby, E. Marmar, M. May, A. Mazurenko, J. Reardon, J. Rice, C. Rost, J. Schachter, J. Snipes, P. Stek, R. Watterson, J. Weaver, B. Welch, and S. Wolfe, in Proceedings of the 16th IAEA Fusion Energy Conference in Montreal, Canada (1997).

[4] R. D. Monk and JET Team, Nucl. Fusion **39**, 1751 (1999).

[5] E. Joffrin, P. Tamain, E. Belonohy, H. Bufferand, P. Buratti, C. Challis, E. Delabie, P. Drewelow, D. Dodt, L. Frassinetti, J. Garcia, C. Giroud, M. Groth, J. Hobirk, A. E. Jarvinen, H.-T. Kim, F. Koechl, U. Kruezi, B. Lipschutz, P. Lomas, E. de la Luna, T. Loarer, P. Maget, C. Maggi, G. Matthews, F. Maviglia, A. Meigs, I. Nunes, G. Pucella, F. Rimini, S. Saarelma, E. Solano, A. Sips, M. Tsalas, I. Voitsekhovitch, H. Weisen, and the JET Contributors, Nucl. Fusion **57**, 086025 (2017).

[6] A. Chankin, E. Delabie, G. Corrigan, C. Maggi, H. Meyer, and JET Contributors, in *Proceedings of the 22nd International Conference on Plasma Surface Interactions, 2016* [Nucl. Mater. Energy **12**, 273 (2017)].

[7] D. Moulton, G. Corrigan, J. Harrison, B. Lipschultz, and JET Contributors, Nucl. Fusion **58**, 096029 (2018).

[8] R. Schneider, H.-S. Bosch, D. Coster, J. Fuchs, J. Gafert, G. Haas, A. Herrmann, M. Kaufmann, A. Kallenbach, J. Neuhauser, J. Schweinzer, U. Wenzel, and ASDEX Upgrade Teams, J. Nucl. Mater. **266-269**, 175 (1999).

[9] A. Kallenbach, M. Kaufmann, D. Coster, J. Fuchs, A. Herrmann, J. Neuhauser, R. Schneider, K. Borrass, H.-S. Bosch, A. Carlson, J. Gafert, K. Lackner, K. Schmidtmann, J. Schweinzer, W. Suttrop, U. Wenzel, and ASDEX Upgrade Team, Nucl. Fusion **39**, 901 (1999).

[10] N. Asakura, N. Hosogane, K. Itami, A. Sakasai, S. Sakurai, K. Shimizu, M. Shimada, H. Kubo, S. Higashijma, H. Takenaga, H. Tamai, S. Konoshima, T. Sugie, K. Masaki, Y. Koide, O. Naito, H. Shirai, T. Takizuka, T. Ishijima, S. Suzuki, A. Kumagai, and JT-60 Team, J. Nucl. Mater. **266-269**, 182 (1999).

[11] S. L. Allen, N. H. Brooks, R. Bastasz, J. Boedo, J. N. Brooks, J. W. Cuthbertson, T. E. Evans, M. E. Fenstermacher, D. N. Hill, D. L. Hillis, J. Hogan, A. W. Hyatt, R. C. Isler, G. L. Jackson, T. Jernigan, C. J. Lasnier, R. Lehmer, A. W. Leonard, M. A. Mahdavi, R. Maingi, W. H. Meyer, P. K. Mioduszewski, R. A. Moyer, D. G. Nilson, L. W. Owen, T. W. Petrie, G. D. Porter, M. E. Rensink, M. J. Schaffer, J. Smith, G. M. Staebler, R. D. Stambaugh, D. M. Thomas, M. R. Wade, W. R. Wampler, J. G. Watkins, W. P. West, D. G. Whyte, N. Wolf, C. P. C. Wong, and R. D. Wood, Nucl. Fusion **39**, 2015 (1999).

[12] S. Allen, J. Boedo, A. Bozek, N. Brooks, T. Carlstrom, T. Casper, R. Colchin, T. Evans, M. Fenstermacher, M. Friend, R. Isler, R. Jayakumar, C. Lasnier, A. Leonard, M. Mahdavi, R. Maingi, G. McKee, R. Moyer, M. Murakami, T. Osborne, R. O'Neill, T. Petrie, G. Porter, A. Ramsey, M. Schaffer, P. Stangeby, R. Stambaugh, M. Wade, J. Watking, W. West, D. Whyte, and N. Wolf, in *14th International Conference on Plasma-Surface Interactions in Controlled Fusion Devices* [J. Nucl. Mater. **290–293**, 995 (2001)].

[13] A. Moser, A. Leonard, A. McLean, H. Wang, and J. Watkins, Nucl. Mater. Energy **19**, 67 (2019).

[14] T. Rognlien, A. McLean, M. Fenstermacher, M. Groth, A. Järvinen, I. Joseph, C. Lasnier, W. Meyer, A. Moser, G. Porter, and U. Umansky, Nucl. Mater. Energy **12**, 44 (2017).

[15] D. Eldon, B. D. Bray, T. M. Deterly, C. Liu, M. Watkins, R. J. Groebner, A. W. Leonard, T. H. Osborne, P. B. Snyder, R. L. Boivin, and G. R. Tynan, Rev. Sci. Instrum. **83**, 10E343 (2012).

[16] T. Carlstrom, C. L. Hsieh, R. Stockdale, D. G. Nilson, and D. N. Hill, Rev. Sci. Instrum. **68**, 1195 (1997).

[17] P. Stangeby, J. Canik, J. Elder, C. Lasnier, A. W. Leonard, D. Eldon, M. Makowski, T. Osborne, and J. Watkins, Nucl. Fusion **55**, 093014 (2015).

[18] A. Leonard, A. McLean, M. Makowski, and P. Stangeby, Nucl. Fusion **57**, 086033 (2017).

[19] G. Porter, J. Moller, M. Brown, C. Lasnier, and DIII-D Team, Phys. Plasmas. **5**, 1410 (1998).

[20] A. Kukushkin, H. Pacher, G. Pacher, G. Janeschitz, D. Coster, A. Loarte, and D. Reiter, Nucl. Fusion **43**, 716 (2003).

[21] A. Kukushkin, H. Pacher, G. Pacher, V. Kotov, R. Pitts, and D. Reiter, J. Nucl. Mater. **438**, S203 (2013).

[22] R. Schneider, X. Bonnin, K. Borrass, D. P. Coster, H. Kastelewicz, D. Reiter, V. A. Rozhansky, and B. J. Braams, Contrib. Plasma Phys. **46**, 3 (2006).

[23] D. Reiter, M. Baelmans, and P. Börner, Fusion Sci. Technol. **47**, 172 (2005).

[24] L. Lao, H. S. John, R. Stambaugh, A. Kellman, and W. Pfeiffer, Nucl. Fusion **25**, 1611 (1985).

[25] L. Casali, C. Sang, A. Moser, B. Covele, H. Guo, and C. Samuell, Contrib. Plasma Phys. **58**, 725 (2018).

[26] L. Casali, "Neutral leakage, power dissipation and pedestal fueling in open vs closed divertors" (unpublished).

[27] P. Stangeby and C. Sang, Nucl. Fusion **57**, 056007 (2017).

[28] A. Leonard, Plasma Phys. Controlled Fusion **60**, 044001 (2018).

[29] M. Groth, G. Porter, M. Rensink, T. Rognlien, S. Wiesen, M. Wischmeier, T. Eich, A. Herrmann, S. Jachmich, C. Lasnier, H. Müller, J. Watkins, M. Beurskens, B. Bray, S. Brezinsek, N. Brooks, M. Fenstermacher, C. Fuchs, A. Huber, A. Kallenbach, A. Leonard, A. Meigs, and D. Rudakov, in *Proceedings of the 19th International Conference on Plasma-Surface Interactions in Controlled Fusion* [J. Nucl. Mater. **415**, S530 (2011)].

[30] J. M. Canik, A. R. Briesemeister, A. G. McLean, M. Groth, A. W. Leonard, J. D. Lore, A. Moser, and BPMIC Team, Phys. Plasmas **24**, 056116 (2017).

[31] R. C. Isler, R. W. Wood, C. C. Klepper, N. H. Brooks, M. E. Fenstermacher, and A. W. Leonard, Phys. Plasmas **4**, 355 (1997).

[32] A. G. McLean, S. L. Allen, M. E. Fenstermacher, A. E. Jaervinen, C. J. Lasnier, G. D. Porter, T. Rognlien, C. M. Samuell, V. A. Soukhanovskii, J. Boedo, E. M. Hollmann, A. W. Leonard, A. L. Moser, D. Thomas, A. Briesemeister, H. Q. Wang, J. D. Watkins, and M. Groth, "Quantification of radiating species in the DIII-D divertor in the transition to detachment using extreme ultraviolet spectroscopy," in *Proceedings of the 27th IAEA Fusion Energy Conference in Gandhinagar, India* (2018), https://conferences.iaea.org/event/151/papers/6065/files/4473-9043_mclean_C7_180926.pdf.

[33] A. Leonard, J. Elder, J. Canik, R. Groebner, and T. Osborne, J. Nucl. Mater. **438**, S246 (2013).

[34] J. Elder, S. Lisgo, A. Leonard, P. Stangeby, J. Boedo, B. Bray, N. Brooks, M. Fenstermacher, D. Reiter, D. Rudakov, E. Unterberg, and J. Watkins, in *Proceedings of the 20th International Conference on Plasma-Surface Interactions in Controlled Fusion Devices* [J. Nucl. Mater. **438**, S651 (2013)].

[35] M. Groth, G. D. Porter, T. D. Rognlien, S. Wiesen, M. Wischmeier, M. N. A. Beurskens, X. Bonnin, B. D. Bray, S. Brezinsek, N. H. Brooks, D. P. Coster, T. Eich, M. E. Fenstermacher, C. Fuchs, R. A. Groebner, D. Harting, A. Huber, S. Jachmich, A. Kallenbach, C. J. Lasnier, A. W. Leonard, A. Meigs, H. W. Müller, M. E. Rensink, D. L. Rudakov, J. G. Watkins, and E. Wolfrum, the DIII-D, ASDEX Upgrade Teams, and JET EFDA Contributors, Plasma Phys. Controlled Fusion **53**, 124017 (2011).

[36] A. Sontag, X. Chen, J. Canik, A. Leonard, J. Lore, A. Moser, M. Murakami, J. Park, and C. Petty, Nucl. Fusion **57**, 076025 (2017).

[37]R. Groebner, M. Mahdavi, A. Leonard, T. Osborne, N. Wolf, G. Porter, P. Stangeby, N. Brooks, R. Colchin, and L. Owen, Nucl. Fusion **44**, 204 (2004).
[38]A. Leonard, M. Groth, G. Porter, and M. Rensink, in *Proceedings of the 18th International Conference on Plasma-Surface Interactions in Controlled Fusion Device* [J. Nucl. Mater. **390–391**, 470 (2009)].
[39]H. Wang, H. Guo, A. Leonard, A. Moser, T. Osborne, P. Snyder, E. Belli, R. Groebner, D. Thomas, J. Watkins, and Z. Yan, and the DIII-D Group, Nucl. Fusion **58**, 096014 (2018).
[40]J. Hughes, B. LaBombard, J. Terry, A. Hubbard, and B. Lipschultz, Nucl. Fusion **47**, 1057 (2007).
[41]M. N. A. Beurskens, T. H. Osborne, P. A. Schneider, E. Wolfrum, L. Frassinetti, R. Groebner, P. Lomas, I. Nunes, S. Saarelma, R. Scannell, P. B. Snyder, D. Zarzoso, I. Balboa, B. Bray, M. Brix, J. Flanagan, C. Giroud, E. Giovannozzi, M. Kempenaars, A. Loarte, E. de la Luna, G. Maddison, C. F. Maggi, D. McDonald, R. Pasqualotto, G. Saibene, R. Sartori, E. R. Solano, M. Walsh, and L. Zabeo, Phys. Plasmas **18**, 056120 (2011).